THE GAS/DUST RATIO OF CIRCUMSTELLAR DISKS: TESTING MODELS OF PLANETESIMAL FORMATION

David Horne[1], Erika Gibb[2], Terrence W. Rettig[3], Sean Brittain[4], David Tilley[3], and Dinshaw Balsara[3]

[1] New York Center for Astrobiology, Rensselaer Polytechnic Institute, 110 Eighth Street, Troy, NY 12180-3590, USA
[2] Department of Physics and Astronomy, University of Missouri—St. Louis, 8001 Natural Bridge Road, St. Louis, MO 63121, USA
[3] Center for Astrophysics, University of Notre Dame, Notre Dame, IN 46556, USA
[4] Department of Physics and Astronomy, Clemson University, Clemson, SC 29634-0978, USA

ABSTRACT

We present high-resolution, near-infrared NIRSPEC observations of CO absorption toward six class II T Tauri stars: AA Tau, DG Tau, IQ Tau, RY Tau, CW Tau, and Haro 6–5b. ^{12}CO overtone absorption lines originating from the circumstellar disk of each object were used to calculate line-of-sight gas column densities toward each source. We measured the gas/dust ratio as a function of disk inclination, utilizing measured visual extinctions and inclinations for each star. The majority of our sources show further evidence for a correlation between the gas/dust column density ratio and disk inclination similar to that found by Rettig et al.

Key words: circumstellar matter – planets and satellites: formation – stars: atmospheres – stars: protostars

1. INTRODUCTION

Classical T Tauri stars (CTTSs) are low-mass young stars surrounded by disks of gas and dust. Planetesimals may eventually form from the materials contained within these disks. Planetesimal formation models indicate that both dust sedimentation and mid-plane turbulence are critical to the formation timescale of planetesimals (Goldreich & Ward 1973; Safronov & Zvjagina 1969; Weidenschilling 1995; Goodman & Pindor 2000; Youdin & Shu 2002; Youdin & Chiang 2004). Greater knowledge of dust and gas evolution can help us to understand the origin and evolution of planetary systems.

In general, circumstellar disks are flared, with a scale height that increases with distance from the central star. Infrared (McCabe et al. 2003; Duchene et al. 2005) and millimeter continuum (Kitamura et al. 2002) observations support evidence for grain growth and settling in these disks. The presence of silicate emission in the mid-infrared is indicative of small (submicron) silicate grains in the hot disk atmosphere (Kessler-Silaci et al. 2006). Strong millimeter continuum observations are evidence of larger, cooler grains at lower scale heights within the disk (Kitamura et al. 2002). Other authors have used SEDs and infrared colors in the mid- to far-infrared, coupled with disk models, to infer that grain growth has occurred (Furlan et al. 2005; D'Alessio et al. 2006). While these observations have provided compelling evidence that grain growth and dust settling has occurred in these systems, the models, color indices, and SED profiles are dependent on, among other things, inclination, mass accretion rate, the degree to which the disk is flared, the clearing of the inner disk, and the assumed dust size distribution and dust opacity.

Other groups have developed theoretical models of disk structure and evolution that take into account turbulence and magnetorotational instability (MRI; Goldreich & Ward 1973; Safronov & Zvjagina 1969; Weidenschilling 1995; Goodman & Pindor 2000; Youdin & Shu 2002; Youdin & Chiang 2004). Recently, Balsara et al. (2009) used their MRI model and an assumed dust size distribution to predict the scale heights of different dust sizes in a minimum solar mass disk model. These models are dependent on the level of turbulent mixing within the disk (Balsara et al. 2009); the level of stratification between dust and gas is a good indicator of this mixing (Rettig et al. 2006).

In this paper, we use high spectral resolution, near-infrared observations of T Tauri stars with known inclinations to directly measure the gas-to-dust ratio at different scale heights. Dust grains residing in the upper disk are thought to undergo growth processes and subsequently settle toward the midplane (Miyake & Nakagawa 1995; Dullemond & Dominik 2004). Consequently, the gas-to-dust ratio at different scale heights in the disk will change, resulting in a higher gas-to-dust ratio in the disk atmosphere and a lower gas-to-dust ratio (dust rich) layer toward the mid-plane.

Rettig et al. (2006) observed the correlation of CO gas column with extinction in a sample of four class II T Tauri stars. These results were used to place constraints on theoretical models of dust settling in circumstellar disks (Balsara et al. 2009). This work extends that sample by a further six sources.

The organization of the paper is as follows. In Section 2, we discuss our observing, reduction, and analysis techniques. In Section 3, we discuss our individual sources, and our resulting conclusions are given in Section 4.

2. DATA REDUCTION AND ANALYSIS

2.1. Observations and Data Reduction

The NIRSPEC spectrometer (McLean et al.1998) mounted on Keck II at the W. M. Keck Observatory, Mauna Kea was used to obtain observations at high resolving power ($\lambda/\Delta\lambda \approx$ 25,000) near-infrared spectra of ^{12}CO ($v = 2$–0) overtone absorption lines near 2.3 μm, toward six class I/II T Tauri stars on 2006 February 17–18. Our observations are summarized in Table 1. Details of our observational and reduction techniques can be found in Brittain et al. (2003) and DiSanti et al. (2001). In short, we observed with a nod pattern that enabled us to cancel telluric lines to first order. The images were then flat-fielded, dark subtracted, and cleaned to remove cosmic-ray hits and hot pixels. Images were then resampled to straighten the spectral and spatial dimensions along rows and columns, respectively. Wavelength calibration and telluric correction were achieved using the GENLN2 atmospheric model (Edwards 1992) in conjunction with the updated HITRAN 2004 molecular database (Rothman et al. 2003, 2005) to generate atmospheric transmittance models at each observed wavelength band.

Table 1
Instrumental Settings for All Sources

Source	Date	Spectral Range (cm^{-1})	Setting/Order	Integration Time (minutes)
DG Tau	2006 Feb 17	4200–4265	K1/32	12
DG Tau	2006 Feb 18	4263–4323	K2/33	4
AA Tau	2006 Feb 17	4200–4265	K1/32	8
AA Tau	2006 Feb 17	4263–4323	K2/33	12
Haro 6–5B	2006 Feb 17	4200–4265	K1/32	16
IQ Tau	2006 Feb 17	4200–4265	K1/32	12
IQ Tau	2006 Feb 18	4263–4323	K2/33	4
RY Tau	2006 Feb 17	4200–4265	K1/32	8
RY Tau	2006 Feb 17	4263–4323	K2/33	12
CW Tau	2006 Feb 17	4200–4265	K1/32	8
CW Tau	2006 Feb 17	4263–4323	K2/33	12

2.2. Removal of Photospheric Absorption Lines

Our targets consist of K and M type stars, which often exhibit significant photospheric CO absorption lines, particularly at the *K* band. Therefore, in order to obtain accurate measurements from only the circumstellar CO contribution, we have expanded our analysis to incorporate the Kurucz theoretical models. Usage of these models to conduct in depth analyses of pre-main-sequence stellar photospheres over the respective gravity ranges covered in this paper is not unusual. The models and procedures employed in this study are based on well-established and accepted methods and have been shown to reproduce high-quality, photospheric signatures in pre-main-sequence stars (see Hauschildt et al. 1999; Doppmann et al. 2005; Najita et al. 2008). Both Doppmann et al. and Najita et al. apply these models to isolate the signature of circumstellar CO in their observations using methods comparable to those presented in this paper.

Synthetic spectra were generated through use of the Moog stellar synthesis program (Sneden 1973) in conjunction with NEXTGEN stellar atmospheric models (Hauschildt et al. 1999) referencing the Kurucz atomic line lists (Kurucz 1979, 1993). The selected models cover a range of temperatures ($T_{\rm eff} =$ 2500–5500 K) and surface gravities (log $g \sim$ 2.5–5.0) at a resolving power equal to that of the observed NIRSPEC data ($\sim$25,000). A least-squares minimization routine was employed to ensure the best possible fit between the observed spectra and the corresponding theoretical model. To accurately reflect the features of the observed spectra, the effects of extinction, rotational broadening, and veiling were incorporated into each model. Atmospheric transmittance was applied to the models in the same manner as the observational data, using the output of the GENLN2 atmospheric model referencing the HITRAN 2004 molecular line database. Values for extinction (A_V), rotational broadening ($v \sin i$), and veiling (r) toward each source were retrieved from the existing literature where available and are summarized in Table 2.

Models were reddened using the same value of A_V employed during the study of disk stratification for each source (see Section 3). Rotational broadening was applied through convolution of the photospheric spectral lines with a line-spread function based on values of $v \sin i$ available in the accepted literature.

After compensation for the above effects, the model spectrum is considered to accurately reflect the "unveiled" spectrum of the target star. Veiling reduces the depth of photospheric lines by enhancing the continuum level of the spectrum; this results in the underestimation of spectral lines' equivalent width. The level of
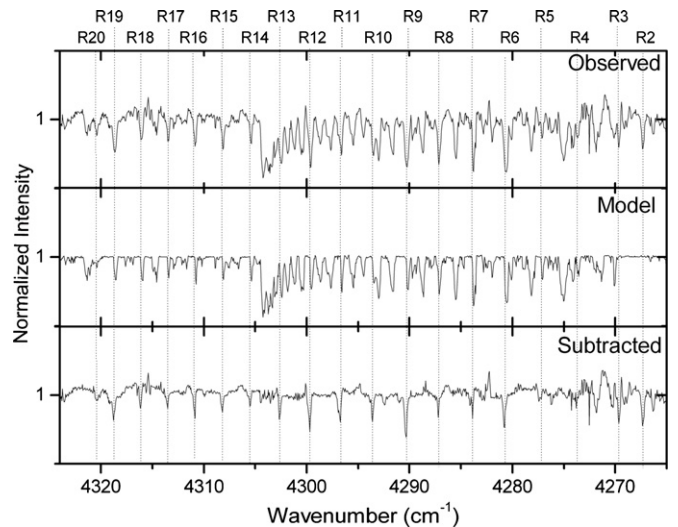

Figure 1. Sampled region of IQ Tau order 33 observational data (top panel), final photospheric model including Doppler shift, $v \sin i$, and veiling corrections (middle panel), and final spectrum produced by subtraction of the photospheric model from the residual (bottom panel). All data have been normalized for comparison purposes.

veiling or veiling factor of a T Tauri star may be quantified as the ratio of the photospheric flux to the flux generated by the surrounding environment:

$$r = \frac{F_{\rm veil}}{F_{\rm phot}}. \qquad (1)$$

In terms of normalized flux, this relates to the equivalent width as

$$1 + r = \frac{W_{\rm phot}}{W_{\rm veil}}. \qquad (2)$$

While we are most likely dealing with an excess of infrared radiation originating from dust in the circumstellar disk, other factors may contribute to veiling in T Tauri stars. The shock region as material falls onto the star increases the local radiation budget, however this effect tends to peak in the ultraviolet. Accretion processes originating in the inner region of the accretion disk may also produce high-energy radiation. We have adopted the method of Hartigan et al. (1989) to determine the degree of veiling in our data. For cases with known veiling, values were applied as an additive constant to the respective model. Veiling estimates were unavailable for Haro 6–5b, therefore this value was determined by incremental variation of the model spectral lines' equivalent widths until a best fit was achieved with the observed data. A constant value was then derived to equalize the depth of the absorption lines in the photospheric model compared to the observed spectrum for each order.

Veiling is relatively constant over small wavelength increments; hence, determination of veiling values on an order-by-order basis minimizes the error budget. The veiling values applied to each source are listed in Table 2. The final model, adjusted for all of the above parameters, was then compared to the observed data for the final time using a least-squares fit to ensure the best possible match to the data. The final models were then subtracted from the observational data, resulting in spectra dominated by circumstellar features. This is illustrated in Figure 1, which shows the original observational data (top panel), the corresponding theoretical photospheric model (middle panel) and the final circumstellar spectrum (bottom panel)

Table 2
Model Input Parameters for Each Source

Source	Inclination (deg)	Applied A_V (mag)	r_K (Veiling 4500 cm^{-1})	$v \sin i$ (km s^{-1})	Estimated Spectral Type (s)	Applied Spectral Type (s)
CW Tau	>80[a]	2.75[b]	3.5[c]	27.4 ± 9.8[d]	K3[a]–K3V[c]	K3
AA Tau	≈75[e]	1.75[b]	0.8 ± 0.4[f]	11.3[g]	K7[a]–M0[h]	K7
IQ Tau	49[f], 71 ± 11[i]	1.44[b]	0.14**[c]	11.5[j]	M0.5[c]–M2[f]	M1
Haro 6-5B	59 ± 14d[i], 67 ± 5[k], 74[l]	10[l]	1.45[*]	20.7 ± 6.4[m]	K5–M4[k]	K5
DG Tau	30[n], 70[o]	1.6[b]	1.4[m]–3.6[j]	22 ± 6[g]	K7–M0[a]	K6
RY Tau	44 ± 5[i], 65[n]	2.2 ± 0.2[b,p]	0.8[q]–2.5[c]	51.6[q]	F8 III[r], K1 IV[s], V[t], G1–G2 IV[u]	G1

Notes.
[*] Value derived from numerical experimentation.
[**] r_k derived from corresponding veiling at adjacent wavelength bands.
References: [a] White & Ghez 2001; [b] Furlan et al. 2006; [c] Folha & Emerson 1999; [d] Bouvier et al. 1999; [e] Schmitt & Robrade 2007; [f] Najita et al. 2003; [g] Bouvier et al. 1999; [h] Calvet et al. 2004; [i] Kitamura et al. 2002; [j] Hartmann & Stauffer 1989; [k] Yokogawa et al. 2001; [l] Stark et al. 2006; [m] Castro & Verdugo 2007; [n] Isella et al. 2010; [o] Kitamura et al. 1996; [p] Muzerolle et al. 1998; [q] Muzerolle et al. 2003; [r] Scherger et al. 2008; [s] Herbig 1977; [t] Cohen & Kuhi 1979; [u] Petrov et al. 1999.

for IQ Tau after removal of the photospheric model. To confirm the accuracy of our method the original data were also analyzed by the fitting of Gaussian profiles to individual photospheric features. The features were then subtracted from the residuals. These results were consistent with the corresponding model subtraction to better than 10%. Accurate matching of spectral features in our method is crucial. We estimate that the maximum error based on the use of a mismatched spectral type will be no more than 0.5–2 spectral subclasses for any given case. For the majority of our sources we assume the values for A_V, $v \sin i$, and veiling quoted in recent literature. Any errors and uncertainties inherent to these values will result from the individual methods used in their determination and would be reflected in our final model.

Given the accuracy of the final fits and accounting for statistical noise along with the factors discussed above, we estimate that the final model fit in any particular case is accurate to 15%, any significant changes to these values would result in an inferior fit. Figures 2(a) and (b) show the reduced spectra produced from our observational data.

2.3. CO Analysis

The CO absorption profile measurements were checked through fitting of a Gaussian profile and by direct integration over each line. We found that both methods gave comparable integrated intensities except in cases where the CO line was blended with another feature. In cases where CO lines are unsaturated (as typically found for the overtone lines near 2.3 μm), the equivalent width (W_ν) is related to the column density in the lower state of the transition (N_J) via

$$W_\nu = (\pi e^2/m_e c^2) N_J f = 8.853 \times 10^{-13} \, N_J f \, (\mathrm{cm}^{-1}), \quad (3)$$

where f is the absorption oscillator strength of the line, calculated from the tables of Goorvitch (1994). Since our absorption lines are not resolved we infer their values by considering the R and P branches separately. For example, the R1 and P1 lines probe the same energy level and should result in column densities that agree. Since they have different oscillator strengths, the line widths can be adjusted until the level populations agree using the value

$$N_J = 66.8 \, b\nu\tau_0 f \, (\mathrm{cm}^{-2}). \quad (4)$$

Population diagrams were used to determine column density and temperature for each of our sources. If we assume that

the circumstellar gas is in local thermodynamic equilibrium the relative population of each energy level can be described by the Boltzmann equation:

$$n_{J''} = (2J'' + 1)e^{-hcBJ''(J''+1)/kT}, \quad (5)$$

where n is the relative population of the energy level, J'' is the lower state rotational quantum number, and B represents the rotational constant. The column density of our CO lines is derived from optically thin lines, therefore no correction for optical depth was necessary. The population diagram for the CO overtone lines of each source, showing the derived rotational temperature and CO column density can be seen in Figure 3.

2.4. The Gas-to-dust Ratio

Rettig et al. (2006) investigated the possibility of a correlation between the measured line-of-sight gas/dust ratio and disk inclination. Observations of gas/dust stratification provide a good measure of internal disk dynamics and the potential for planetesimal formation. If gas and dust are well mixed in the disks of YSOs (D'alessio et al. 1999), it may be assumed that the ratio of column density to extinction [$N(\mathrm{CO})/A_V$] is independent of viewing angle. If dust in disks preferentially settles toward the midplane then there should be a correlation between $N(\mathrm{CO})/A_V$ and inclination. A reduction in extinction due to dust levels should be observed along the line of sight toward a face-on disk ($i \approx 0°$), resulting in larger values of $N(\mathrm{CO})/A_V$ when compared to a disk viewed close to the midplane ($i \approx 90°$), where $N(\mathrm{CO})/A_V$ will approach the interstellar value [$N(\mathrm{CO})/A_V$]$_{\mathrm{interstellar}}$. We adopted the accepted value of [$N(\mathrm{CO})/A_V$]$_{\mathrm{interstellar}} = 1.4 \times 10^{17}$ cm^2 mag^{-1}, calculated from the interstellar CO/H$_2$ abundance ratio of 1.56×10^{-4} with $A_V/N(\mathrm{H_2}) = 10.8 \times 10^{-22}$ mag cm^{-2} (Mathis 1990; Kulesa 2002). This value was used to normalize our observed line-of-sight measurements of the $N(\mathrm{CO})/A_V$ ratio. This gives the expression $\Delta = [N(\mathrm{CO})/A_V]_{\mathrm{disk}}/[N(\mathrm{CO})/A_V]_{\mathrm{interstellar}}$. The value of Δ provides an effective measure of the difference between the [$N(\mathrm{CO})/A_V$] contribution from the source compared to the ISM; our aim is to calculate the value of Δ for each observed source.

Once the temperature and column density of ^{12}CO along the line of sight to each source were determined, the gas-to-dust ratio could be calculated and compared to values from Rettig et al. (2006). The amount of dust along the line of sight was inferred using the extinction (A_V), where the values of A_V are found in existing literature and are derived
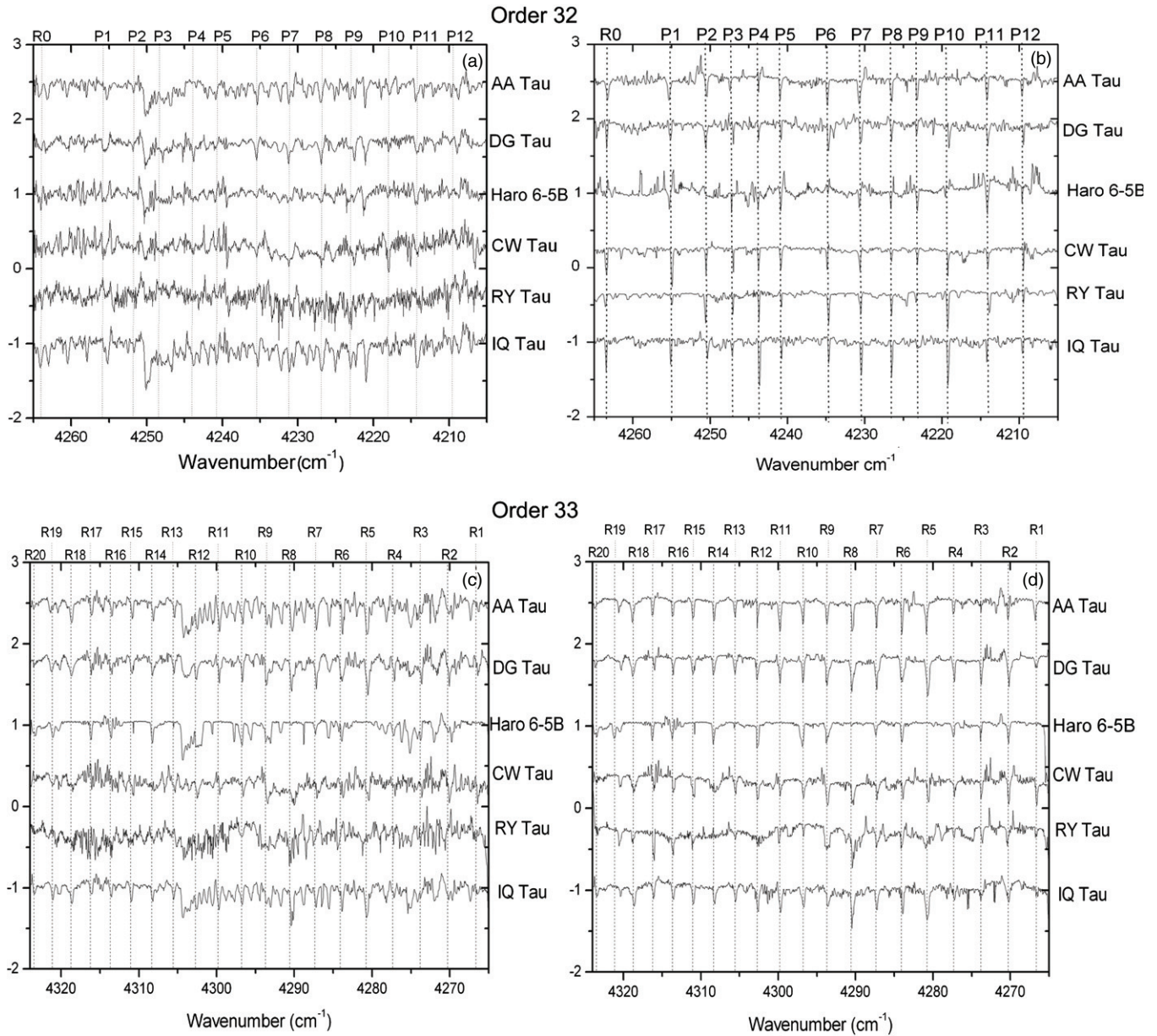
Figure 2. K-band spectra showing ^{12}CO $v = 2$–0 overtone lines for six sources. Spectra have been compensated for Doppler shift, normalized and vertically shifted for comparison purposes. The locations of prominent ^{12}CO absorption features are marked by vertical dotted lines. (a) K-band order 32 observed data, (b) K-band order 32 with the stellar photosphere removed, (c) K-band order 33 observed residual spectra, and (d) order 33 with the stellar photosphere removed.

from common optical and NIR (*JHK*) photometry methods (see Table 2). These $[N(\mathrm{CO})/A_V]_{\mathrm{disk}}$ values are then compared to the interstellar $[N(\mathrm{CO})/A_V]_{\mathrm{interstellar}}$. Following the procedure of Rettig et al. (2006), we utilized the same ratio of $[N(\mathrm{CO})/A_V]_{\mathrm{source}}/[N(\mathrm{CO})/A_V]_{\mathrm{interstellar}} = \Delta$ and compared the variation of Δ with the inclination of the source. All derived values of $T(\mathrm{CO})$ and Δ along with those found by Rettig et al. (2006) are shown in Table 2 and discussed in Section 3. Figure 4 shows a comparison of the Δ values calculated for the six new sources compared to inclination values available from current literature. This figure also encompasses data from of the Rettig et al. (2006) survey.

In some cases more than one discrete inclination value is listed for an individual source (see Tables 1 and 2). In order to ascertain the overall effect of these alternate values on any Δ:inclination relationship that may exist, a series of linear fits were applied to the data in Figure 4. These fits were calculated for every

combination of inclination value, including alternate values for the same source. Each of these fits is shown as in Figures 4(a) and (b), these trends follow a relatively tight correlation with respect to one another. Including AA Tau in our sample (Figure 4(a)) results in linear fits covering a range from $\Delta = 9.9$ to 13.8 at an inclination of $90°$. Excluding AA Tau results in a far tighter distribution covering a Δ range of 1.2, from $\Delta = 5.2$ to 6.4 at inclination $= 90°$ (Figure 4(b)).

This indicates that any differences in the Δ:inclination trends resulting from the use of alternate inclination values are relatively small compared to the overall spread of the datapoints. AA Tau was neglected from the fits shown in Figure 4(b) to demonstrate the overall relationship in the absence of this extreme outlier. The removal of AA Tau from the data set results in a tighter fit to the remaining points along with a shallower gradient and a reduction of the *y*-axis intercept of approximately 50%.
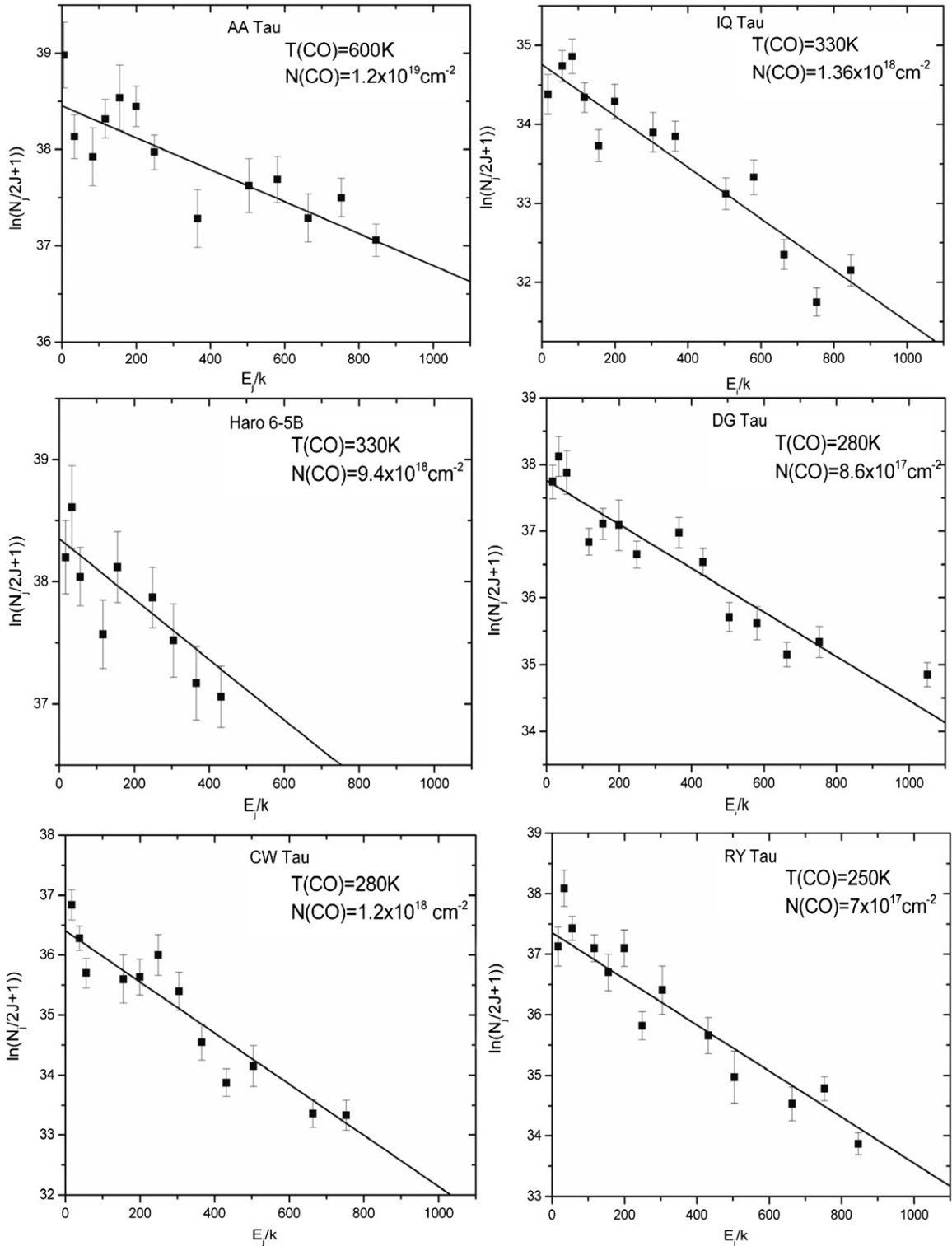
Figure 3. Population diagrams of ^{12}CO (2–0) overtone absorption lines based on K band order 32 and order 33 measurements for all six sources.

3. MODEL INPUT PARAMETERS AND RESULTS

1. AA Tau is a 0.8 $M_\odot$ K7 (Muzerolle et al. 1998) star inclined by $i \approx 75°$ (Bouvier et al. 1999). Extinction toward AA Tau is about $A_V \approx 1.75$ (Furlan et al. 2006). AA Tau is accreting material with a value of between $\dot{M} = 10^{-7}$ $M_\odot$ yr^{-1} (Hartigan et al. 1995) to 10^{-8} $M_\odot$ yr^{-1} (Muzerolle et al. 1998) and is known to undergo variations in brightness of up to 1.2 mag over an 8.22 day period (Bouvier et al. 2007).

The level of veiling also varies from 0.2 to 0.7 over this period. The magnitude variations are believed to result from periodic eclipses caused by the magnetically warped inner disk (Bouvier et al. 2003). It has been estimated that the extinction toward AA Tau increases by up to an order of magnitude depending on the position of this inhomogeneity (Stark et al. 2006).

Long-duration studies of AA Tau have detected changes to the magnetospheric structure of the star over a period of several
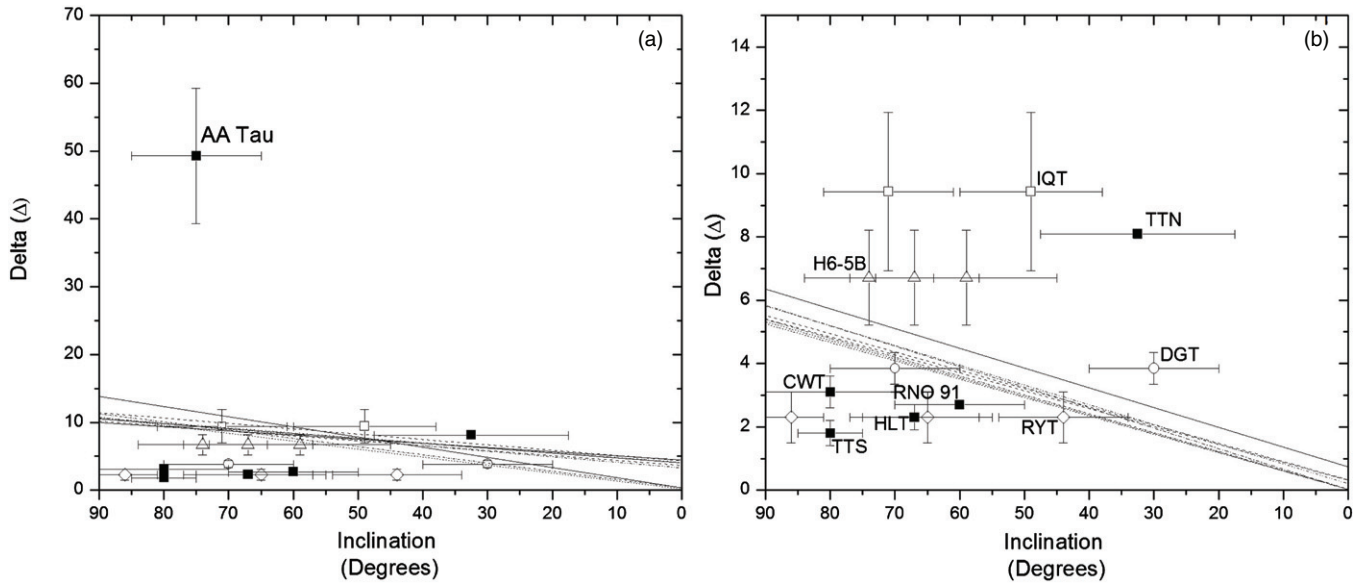
Figure 4. (a) Disk inclination compared to Δ for all surveyed sources including data from Rettig et al. (2006) with linear fits applied for all combinations of alternative inclination values. All sources are labeled on diagram: solid symbols indicate objects with single inclination value. Open symbols indicate objects with multiple inclination values—square: IQ Tau; triangle: Haro 6–5B; circle: DG Tau; and diamond: RY Tau. Note the elevated Δ for AA Tau. (b) Close-up view of inclination compared to Δ for seven sources seen in panel (a) from inclination $= 50^\circ$ to 90°. Linear fits are applied for each possible combination of alternative inclination values. AA Tau is omitted from the linear fits in panel (b).

years (Bouvier et al. 2007). Rotationally modulated hot spots have also been observed as material falls onto the central star (Bouvier et al. 2007).

Analysis of AA Tau's optical spectrum (Hirth et al. 1997) along with direct imaging (Cox et al. 2005) has confirmed the presence of jets in this system. AA Tau exhibits a very high Δ value of 59.5, a departure from the general trend of Figure 4. CO temperatures were elevated (600 K) toward AA Tau. Given the high value of $N(\text{CO}) = 1.2 \times 10^{19}$ cm^{-2} coupled with high $T(\text{C}^{18}\text{O})$, it is possible that gas within the disk is inflated to greater scale height and we are observing hot CO gas present in the inflated disk.

This high temperature is consistent with the increased radiation field heating the gaseous material in the disk through enhanced magnetospheric accretion (Bouvier et al. 2007); however, temperature enhancement is not apparent among more strongly accreting objects in our sample. It is possible that secondary heating from local hot spots located on the star's surface may contribute to an increase in gas temperature. Our observations may have sampled a warmer inhomogeneity in the disk, resulting in elevated CO temperature readings compared to the disk as a whole.

2. Haro 6–5B is a 0.2 $M_\odot$, K5 star with a circumstellar disk inclined by 59° (Kitamura et al. 2002), $67^\circ \pm 5^\circ$ (Yokogawa et al. 2001), or alternately by 74° (Stark et al. 2006). Yokogawa et al. also indicate that Haro 6–5B possesses an active structured jet system and is in a transitional phase between a class I and class II object, having dissipated its surrounding envelope. This is supported by Stark et al. (2006) who also found no evidence of an envelope, but suggested that Haro 6–5B is subject to extinction by a host molecular cloud. Based on near IR color observations and the results of light scattering models, extinction toward Haro 6–5B is determined to be $A_V \approx 10$ (Stark et al. 2006; Scherger et al. 2008). Information on the level of veiling toward Haro 6–5b was unavailable; therefore, a best-fit value of 1.2 was determined through modeling of the observed spectral features (see Section 2.1).

We measured $N(\text{CO})$ to be 1.2×10^{19} cm^{-2}, giving a value of $[N(\text{CO})/A_V]_{\text{disk}} = 4.1 \times 10^{17}$ cm^{-2} mag^{-1}. Using the value of $A_V \approx 10$ we determine that $\Delta = 6.7$, a value slightly higher than the established trend of Rettig et al. (2006). This Δ is relatively consistent with the 59°–67° inclination angles proposed by Kitamura et al. and Yokogawa et al.

3. IQ Tau is a 0.52 $M_\odot$, M0.5–M2 star (Kitamura et al. 2002). Reported disk inclinations for this source vary: Kitamura et al. (2002) reports a value of 71°; more recently, Najita et al. (2003) determined a much lower value of $i \approx 49^\circ$ based on the rotational period and $v \sin i$ of the source. The potential effects of this alternate value are shown by the linear fits applied in Figures 4 and 6. The accretion rate of IQ Tau is estimated to be around 10^{-8} $M_\odot$ yr^{-1} (Muzerolle et al. 1998) with an extinction of $A_V \approx$ 1.44 (Furlan et al. 2006). We derived a column density of 1.9×10^{18} cm^{-2} for $N(\text{CO})$ toward IQ Tau; this corresponds to a value of $[N(\text{CO})/A_V]_{\text{disk}} = 1.3 \times 10^{18}$ cm^{-2} mag^{-1}. The enhanced CO column density toward IQ Tau results in a slightly elevated value of $\Delta = 9.4$, which may suggest a relatively "face-on" orientation respect to the observer.

4. DG Tau is a 1 $M_\odot$ CTTS encompassed by a relatively compact circumstellar disk composed of gas and dust (Testi et al. 2002), with inclinations of between 30° (Isella et al. 2010) and 70° (Hessman & Guenther 1997). Estimated spectral types range from K5 to M2. The final fitted spectral type was found to be K6, consistent with Hessman & Guenther (1997). DG Tau has a relatively high accretion rate of around 10^{-6} (Muzerolle et al. 1998) to 2×10^{-7} $M_\odot$ yr^{-1} (Hartigan et al. 1995), strong well-structured jets with discernable knots have also been observed (Dougados et al. 2000). Extinction estimates toward DG Tau are estimated at $A_V \approx 1.6$ (Furlan et al. 2006). We determined a CO column density of 2.6×10^{17} cm^{-2}, giving $[N(\text{CO})/A_V]_{\text{disk}} = 5.4 \times 10^{17}$ and $\Delta = 3.85$.

5. RY Tau is a 2.37 $M_\odot$ (Kitamura et al. 2002) star and evidence exists to suggest that it is a binary system (St-Onge & Bastien 2008). Several discrete inclination values are quoted in the literature for RY Tau: $i \approx 44^\circ$ (Kitamura et al. 2002),

$i \approx 48°$ (Yokogawa et al. 2001), using photometric observations, with a further value of $i \approx 65°$ derived through thermal dust emission mapping (Isella et al. 2010). A distinctive jet and counterjet have been observed extending out to around $31''$ and $3.5'$, respectively (Onge & Bastien 2008). RY Tau has been known to vary in brightness by as much as two orders of magnitude in the visual to NIR wavelengths. These variations have been attributed to obscuration of the central star by knots in the circumstellar disk and/or envelope (Eiroa et al. 2002). There is also some uncertainty reported in the existing literature as to the exact spectral type of RY Tau. Herbig (1977) and Cohen & Kuhi (1979) both considered RY Tau to be a K1 star, whereas Holtzman et al. (1986), Cabrit et al. (1990), and Petrov et al. (1999) report spectral types ranging from G1-G3 IV. More recent observations by Eiroa et al. (2002) and Scherger et al. (2008) designate RY Tau as an F8 III star. We found that the best fit to our observations was achieved with a G1 model spectrum, in agreement with Petrov et al. Extinction estimates toward RY Tau also vary from 1.3 (Kuhi 1974) to 2.7 mag (Beckwith et al. 1990). We have adopted the value of $A_V \approx 2.2$ mag determined by Furlan et al. (2006) from IR color observations. We determined a value of $N(CO) = 7.0 \times 10^{17}$ cm^{-2}, corresponding to $[N(CO)/A_V]_{disk} = 3.2 \times 10^{17}$. This results in a Δ of 2.3, given an inclination of $\approx 65°–70°$, the Δ value of RY Tau correlates well with the sources DG Tau (assuming $I \approx 70° \pm 10°$) and HL Tau ($i \approx 67° \pm 10°$) (Rettig et al. 2006) as shown in Figure 4.

6. CW Tau is a K3, $1.06 M_\odot$ star with active structured jets (Dougados 2008) and an inclination of $\approx 80°$ (White & Ghez 2001) and is accreting at a rate of around $10^{-6} M_\odot$ yr^{-1} (Hartigan et al. 1995). CW Tau has been known to vary in brightness by as much as two orders of magnitude in visual to NIR wavelengths, these variations have been attributed to obscuration of the central star by knots in the circumstellar disk and/or envelope (Eiroa et al. 2002). Extinction toward this source is estimated to be around $A_V \approx 2.75$ mag (Furlan et al. 2006). The CO column density was found to be $N(CO) = 1.8 \times 10^{18}$ cm^{-2}, giving $[N(CO)/A_V]_{disk} = 1.1 \times 10^{17}$ cm^{-2} mag^{-1} resulting in $\Delta = 3.1$, which is reasonably consistent with the estimated inclination of $\approx 80°$. The slightly elevated temperature of the CO gas toward CW Tau is likely due to an increase in the local radiation field resulting from the active accretion of this source. Alternatively, inhomogeneities within the disk could be influencing our observations of the circumstellar CO gas as with AA Tau.

The parameters of the final fitted models for each of the above cases are summarized in Table 3.

4. COMPARISON WITH THEORETICAL MODELS

Theoretical models of dust/gas ratios were generated by Rettig et al. (2006) for comparison with observational data. These models are tested here against the updated sample of circumstellar disk observations. The models employ an α disk formulation to evaluate dust-settling times within the disk. A range of values from $\alpha = 1.5 \times 10^{-5}$ to 1.25×10^{-3} were used to evaluate dust settling times, with the assumption that the temperature within the disk varies as a function of radius (D'Alessio et al. 1998). Values of α were determined from a best fit of the models to the observed data, with initial values estimated from the observed accretion rates of each sources. In this treatment, α values reflect the level of turbulence within the disk, where a lower α corresponds to a system in a quiescent state.

These models incorporate the Mathis et al. (1977, MRN) power-law distribution in a quasi-steady state with an initial gas/dust ratio equal to that of the interstellar medium. These models were combined with estimates of dust grain opacity for grains of varying size from 0.1 to $10 \,\mu$m (Draine & Lee 1984), allowing the expected dust/gas ratio (Δ) to be calculated along the line of sight toward each disk. Dust grain growth is incorporated through a reduction in the MRN power-law index, while holding the overall mass of the system constant. (See Rettig et al. 2006 for a complete discussion of the methods used in these models and their implementation.)

Model results are expressed as a function of inclination in the same manner as the observed values in Figure 4. The power-law trend was adjusted through variation of both α and dust grain size until a best fit to the observational results was achieved. Figure 5 shows comparisons of the theoretical trend in gas/dust ratio with inclination for the updated sample of observations.

Figure 5(a) shows a fit to the observed data by the theoretical trend produced for dust with radii of $0.1 \,\mu$m to 1 cm; this yields a slope of -3.42 in the power-law dust number density distribution (where a value of -3.5 is used for an MRN dust distribution). Extremely low values of α ($\approx 5 \times 10^{-5}$) were required to fit the observed distribution, suggesting that the assumed dust grain size in this case was too large. To accommodate this, the power-law fits of Figure 5(b) incorporate elevated levels of grain growth. Dust grain sizes were increased to between $1 \,\mu$m and 1 cm, with a density distribution of -3.4. Adjustment of these parameters resulted in an increase in the level of turbulence, inflating α values by a factor of ~ 10.

The third and final case, shown in Figure 5(c), incorporates dust sizes ranging from $3 \,\mu$m to 1 cm with a density distribution of -3.37 and $\alpha \approx 10^{-3}$. The overall distribution is best fit by the $\alpha = 1.25 \times 10^{-3}$ trend and with the obvious exception of AA Tau, values are neatly bracketed by the corresponding upper and lower alpha values of 2×10^{-3} and 4.5×10^{-3}.

The α values used in the determination of Figure 5(c) are more consistent and physically reasonable with respect to the earlier findings of Rettig et al. (2006). However, the addition of the new data set results in a steeper relation between Δ and inclination than originally found in Rettig et al. The power-law dust density distribution of -3.37 required to fit the updated observational sample seen in each plot represents a significant deviation from the original smaller Rettig et al. survey, which closely followed the classical MRN distribution of -3.5.

The model fits to the increased observational sample; specifically, those of Figure 5(c) suggest that greater levels of turbulence and dust grain growth may be at work in these disks than indicated by the original sample of four objects. Increases in turbulence along with higher density factors are key in the promotion of dust particulate growth (Weidenschilling 1977) and may indicate a greater potential for planetesimal formation than originally thought.

A discussion of the implication of these model fits on the perceived physical parameters of the disk and their potential meaning with respect to the observational data is given in the following section.

5. DISCUSSION

Rettig et al. (2006) found that the enhancement of gas relative to dust correlated with disk inclination in a set of four class II T Tauri stars. The correlation could be reproduced in a theoretical disk model with nonzero turbulent velocity and by
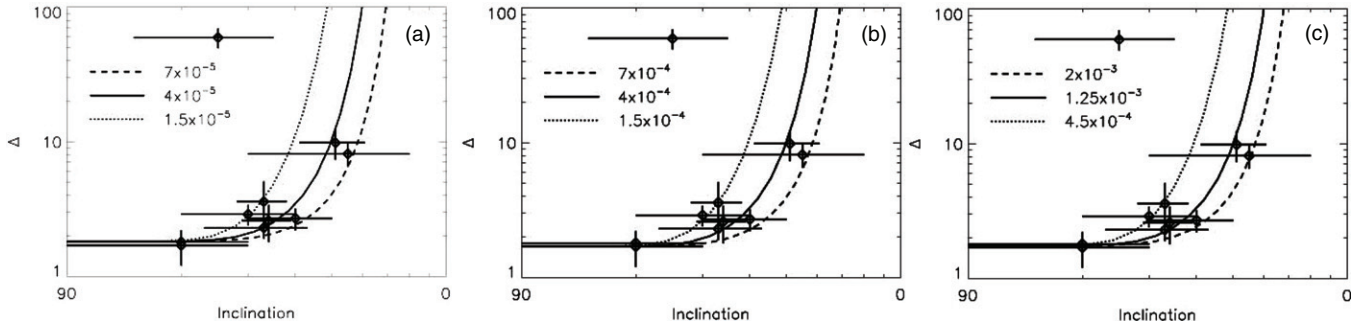
Figure 5. Theoretical Δ:inclination power-law fits to observational data. (a) Dust size distribution from $0.1\,\mu$m to 1 cm with power-law number density $= -3.42$. (b) Dust size distribution from $1\,\mu$m to 1 cm with power-law number density $= -3.4$. (c) Dust size distribution from $3\,\mu$m to 1 cm with power-law number density $= -3.37$. The value of α for each case is given on the respective graph, where α is the viscosity prescription of the disk. Symbols represent the observationally determined values of Δ for comparison with the theoretical trends.

<div align="center">

Table 3
Final Quantities Selected or Derived for Each Source Based on Final Results

</div>

Source	Inclination (deg)	A_V	Disk $N(CO)/A_V$ (cm^{-2} mag^{-1})	$N(CO)$ (cm^{-2})	$T(CO)$ (K)	Δ
TTauS[*]	>80	35	$2.6 \pm 0.4 \times 10^{17}$	$9.0 \pm 0.3 \times 10^{18}$	100–300	1.8 ± 0.4
CW Tau	>80[a]	2.75[i]	$4.4 \pm 0.5 \times 10^{17}$	1.2×10^{18}	≈ 280	3.1 ± 0.5
AA Tau	$\approx 75 \pm 10$[b]	1.75[i]	$6.9 \pm 0.2 \times 10^{18}$	1.2×10^{19}	≈ 600	49.3 ± 10
IQ Tau	49[c], 71 ± 11[d]	1.44[i]	$1.3 \pm 0.4 \times 10^{18}$	$1.9 \pm 0.3 \times 10^{18}$	≈ 300	9.4 ± 2.5
Haro 6-5B	59 ± 14[d], 67 ± 5[e], 74[f]	10[f]	$9.4 \pm 0.7 \times 10^{17}$	9.4×10^{18}	≈ 330	6.7 ± 1.5
DG Tau	30[g], 70 ± 10[h]	1.6[i]	$5.4 \pm 0.5 \times 10^{17}$	8.6×10^{17}	≈ 280	3.85 ± 0.5
RY Tau	44[d], 65[g]	2.2 ± 0.2[i,j]	$3.2 \pm 0.6 \times 10^{17}$	7.0×10^{17}	≈ 250	2.3 ± 0.8
HL Tau[*]	67 ± 10	24	$3.2 \pm 0.5 \times 10^{17}$	$7.5 \pm 0.2 \times 10^{18}$	≈ 100	2.3 ± 0.4
RNO91[*]	60 ± 10	9	$3.8 \pm 0.7 \times 10^{17}$	$3.3 \pm 0.2 \times 10^{18}$	≈ 50	2.7 ± 0.5
TTauN[*]	20-45	1.5	$1.2 \pm 0.2 \times 10^{18}$	$1.7 \pm 0.1 \times 10^{18}$	≈ 100	8.1 ± 1.54

Notes.
[*] Rettig et al. 2006; [a] White & Ghez 2001; [b] Schmitt & Robrade 2007; [c] Najita et al. 2003; [d] Kitamura et al. 2002; [e] Yokogawa et al. 2001; [f] Stark et al. 2006; [g] Isella et al. 2010; [h] Kitamura et al. 1996; [i] Furlan et al. 2006; [j] Muzerolle et al. 1998.

modifying the MRN dust distribution to allow for grain growth (see also Balsara et al. 2009).

The ability of dust to settle to the midplane of the disk is determined by the level of turbulence and the gravity of the disk. Tilley et al. (2010) found that dust settles more efficiently in the outer disk due to weaker turbulence and lower gas density. In their model, the scale heights for small (micron) sized dust grains follow the gas scale heights through much of the inner disk and begin to drop dramatically for larger dust grains. Such an effect should be observationally detectable as an enhanced gas/dust ratio as inferred by Rettig et al. (2006). In this work, we investigated an additional six objects of similar class (and hence evolutionary state) to see if the correlation between the gas/dust ratio and inclination holds for a larger number of sources.

For most of our sources (Figure 4) we find that in general, as the disk becomes more face-on, the gas/dust ratio in the disk, $[N_{CO}/A_V]_{disk}$, increases relative to the interstellar value. This suggests that a significant amount of dust settling has occurred in the uppermost disk of these objects.

Given the geometry of these objects, it is likely we are sampling material at varying depths and radii within the disk as a function of inclination. As a result it becomes more difficult to draw conclusions as to the level of dust settling deep within the disk for sources with $i > 60°$ due to the propensity for backscattering of light from the far side of the disk. This form of interference from scattering is inherent to observations of class I–class II objects such as these (Whitney et al. 2003).

Due to this effect we only draw firm conclusions as to the level of dust settling in the uppermost parts of the disk. Also, our method may not be used to infer the inclination of a source, as other characteristics such as evolutionary state and disk atmosphere heating by the central star may also influence the gas/dust ratio in an object.

The effects of backscattered radiation within the disk may also be somewhat responsible for the relatively wide distribution of points at higher inclination values seen in the inclination: $[N_{CO}/A_V]_{disk}$ and inclination:Δ relationships.

For Haro 6–5B, there is some evidence that this object is in transition from a class I–class II object (Yokogawa et al. 2001). If we accept the higher value of A_V in Table 2 (which would be in keeping with a class I or earlier class II object), then the Haro 6–5B Δ agrees with those for other objects of comparable inclination. Both Haro 6–5B and HL Tau share similar physical characteristics; this may suggest that HL Tau is in a similar class I–class II transitional state to Haro 6–5B. A similar relationship may exist between DG Tau and RY Tau in the new sample of sources. IQ Tau and AA Tau also share very similar physical parameters; however, the high gas temperatures and elevated $N(CO)$ observations in the case of AA Tau are likely due to differences in the local environment caused by either magnetospheric activity or secondary heating of the disk of AA Tau and not an indication of an evolutionary trend. It is difficult to discern if the differences observed in our sample are due to the relative evolutionary state of the respective sources or due to natural diversity of the initial conditions of each disk. Greater knowledge of the evolutionary state of our sources would be
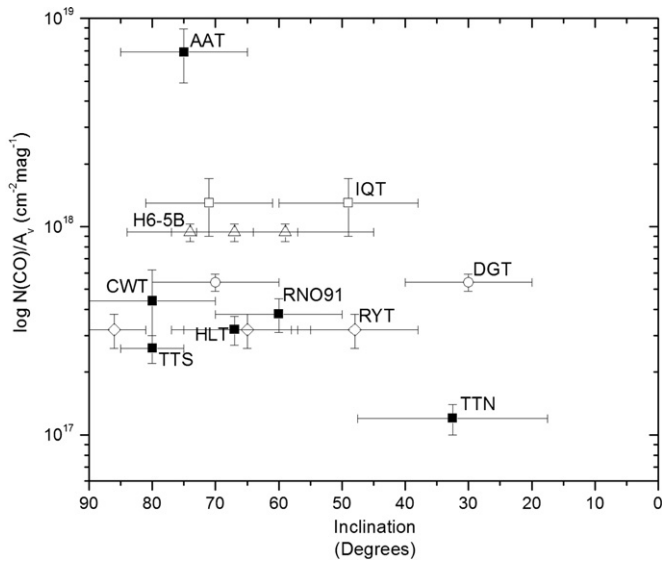
Figure 6. Correlation of inclination with $N(CO)/A_V$. All sources are labeled on the diagram; solid symbols indicate objects with single inclination values. Open symbols indicate objects with multiple inclination values—square: IQ Tau; triangle: Haro 6–5B; circle: DG Tau; and diamond: RY Tau.

advantageous along with a greater sample of sources with gas/dust ratio measurements.

One object, AA Tau, differed significantly from the others in our study. It has a much higher gas column density than the other sources. We note that AA Tau has a significantly higher CO rotational temperature than the other sources (Table 3). AA Tau is highly variable with a magnetically warped disk (Bouvier et al. 2003) and active accretion. Thus, the enhanced gas/dust ratio may be due to the increased scale height of the gas resulting from the enhanced temperature.

It is possible that anomalous Δ values may result from inaccuracies in the observed disk inclinations for YSOs. It has been shown that YSOs may project a disk shadow (Hodapp et al. 2004), which can lead to ambiguities when attempting to determine the size and morphology of YSOs. This effect may limit the accuracy to which the disk orientation may be determined.

Figure 6 shows the inclination of each source compared to their respective column densities of $N(CO)/A_V$. Sources with inclinations between 60° and 75° appear to have similar values of $N(CO)/A_V$, either close to or within their respective $N(CO)$ errors (see Table 2). In general, the $N(CO)/A_V$:inclination ratio behaves very similarly to the Δ:inclination plot. This is due to the dominance of the $N(CO)/A_V$ in the calculation of Δ. A possible future extension may be to better constrain the inclination and the physical environment of the YSO through Monte Carlo modeling (Pontoppidan et al. 2005) of disk shadow effects in cases exhibiting anomalous $N(CO)$:inclination values.

The agreement between the alpha disk model trends and the observed Δ values is surprisingly good in this regime (see Figures 5(a)–(c)). Very low values of α were required as input to the α disk formulation models to adequately describe the observed distribution in Δ. It is likely that the alpha values employed to fit our data set, are inconsistent with the observed accretion rates for these objects (as a more turbulent disk would be required to transport angular momentum).

One possible explanation for the perceived dichotomy in the α:accretion rate may be that our observed dust-to-gas ratio is preferentially sensitive to the more quiescent outer disk. Therefore α may tend to a lower value for the outer disk, whereas the observed accretion rates for these objects may originate in the far more turbulent inner disk.

It is possible to scale our models to match the observational trend utilizing alternative α values in the 10^{-3} to 10^{-4} range. However, this change in α would also require a corresponding increase in the minimum dust grain size to $\approx 10\,\mu$m. Dust grains of this size are not likely to have been observed in our data set; therefore, we are forced to adopt the lower range of $\alpha \approx 10^{-3}$ to 10^{-4} to remain consistent with our observed quantities.

6. CONCLUSIONS

These results show further positive evidence of gas/dust stratification in the disks of YSOs, more than doubling our statistical sample of these measurements from four to ten.

Five of the six new sources: CW Tau, DG Tau, RY Tau, IQ Tau, and Haro 6–5B fit the trend between the $[N(CO)/A_V]$ and inclination established by Rettig et al. (2006). A disk exhibiting a more "face-on" orientation will possess a higher $[N(CO)/A_V]$, while a disk observed toward the midplane will have an $[N(CO)/A_V]$ approaching the interstellar value. This effect results in the contrasting values of Δ based on disk inclination observed in our data set.

High-resolution theoretical stellar models were used to successfully remove the photospheric contribution of the background star to the observed spectrum, improving our observations of circumstellar material.

Haro 6–5b, a class I/II transition object fits well with the established gas/dust ratio: inclination trend. The dependence of $[N(CO)/A_V]$ and the corresponding Δ value on the evolutionary state of the YSO is inconclusive given the size of the current sample.

Based on a comparison of the physical attributes of Haro 6–5B and HL Tau it is possible that HL Tau may be an early class II or transitional object.

Comparison of the updated observational results with theoretical model outputs identifies a deviation in the power-law dust density distribution from the standard MRN value established in Rettig et al. (2006). The form of the dust density distribution is consistent with dust grain growth. The result of the α disk formulation simulations suggest that typical dust grain sizes are on the order of $\sim 3\,\mu$m–1 cm. Evidence for dust grain growth has been observed at millimeter wavelength scales toward circumstellar disks of T Tauri stars (D'Alessio et al. 2001).

Due to the effects of scattering discussed in Section 5, it is difficult to quantify the level of dust settling deep within the disk, we are however confident that our results may provide insight into dust settling in the upper disk. This may assist in future gas line and continuum emission models of these objects (Woitke et al. 2010).

Theoretical fits to the updated Δ:inclination distribution indicate that both turbulence and dust density in these disks may be at higher levels than originally thought. Observations of the size and distribution of dust grains within the circumstellar disk along with estimates of turbulence within the disk environment provide further constraints for planetary formation models.

We have identified that our theoretical models require quite low values of α to adequately describe the observed range in Δ. This may indicate that the outer regions of the disk may be more quiescent than previously thought. This suggests that accretion

in these sources is heavily localized in the vicinity of the star and not at work in the outer disk.

7. FUTURE WORK

A larger sample will be required to truly judge any dependence between the gas/dust ratio and the evolutionary status of the source. Statistically, our sample only represents a small sample of known YSOs surveyed for the effects of dust stratification and observations of this effect in a greater number of cases are needed.

The majority of our sources also possess inclinations greater than 60°; a wider ranging sample of disk-bearing systems with inclinations below this value would be advantageous. Better constraints on the evolutionary status and inclination of the target sources would assist studies of this type and updates may be made to this work if better inclination determinations become available in the future. Incorporation of models to discern the effect of disk shadows in anomalous sources would assist in the characterization of the physical conditions and orientation of these sources. Greater understanding of disk dynamics and incorporation of these effects into our models is required.

Finally, AA Tau itself is a source worthy of further observations, to increase our understanding of its dynamic circumstellar environment.

REFERENCES

Balsara, D. S., Tilley, D. A., Rettig, T., et al. 2009, MNRAS, 397, 24
Beckwith, S. V. W., Sargent, A. I., Chini, R., & Gusten, R. 1990, AJ, 99, 924
Bouvier, J., Alencar, S. H. P., Boutelier, T., et al. 2007, A&A, 463, 1017
Bouvier, J., Chelli, A., Allain, S., et al. 1999, A&A, 349, 619
Bouvier, J., Grankin, K. N., Alencar, S. H. P., et al. 2003, A&A, 409, 169
Brittain, S. D., Rettig, T. W., Simon, T., et al. 2003, ApJ, 588, 535
Cabrit, S., Edwards, S., Strom, S. E., et al. 1990, ApJ, 354, 687
Calvet, N., Muzerolle, J., & Briceño, C. 2004, AJ, 128, 1294
Castro, A. I., & Verdugo, E. 2007, ApJ, 654, 91
Cohen, M., & Kuhi, L. V. 1979, ApJS, 41, 743
Cox, A. W., Hilton, G. M., & Williger, G. M. 2005, BAAS, 37, 1287
D'Alessio, P., Calvet, N., & Hartmann, L. 2001, ApJ, 553, 321
D'Alessio, P., Calvet, N., Hartmann, L., Lizano, S., & Cantó, J. 1999, ApJ, 527, 893
D'Alessio, P., Calvet, N., Hartmann, L., et al. 2006, ApJ, 638, 314
D'Alessio, P., Canto, J., Calvet, N., & Lizano, S. 1998, ApJ, 500, 411
DiSanti, M. A., Mumma, M. J., Dello Russo, N., et al. 2001, Icarus, 153, 361
Doppmann, G. W., Greene, T. P., Covey, K. R., et al. 2005, AJ, 130, 1145
Dougados, C. 2008, Lecture Notes in Physics, Vol 742 (Berlin: Springer)
Dougados, C., Cabrit, S., Lavalley, C., et al. 2000, A&A, 357, L61
Draine, B. T., & Lee, H. M. 1984, ApJ, 285, 89
Duchene, G., Ghez, A. M., McCabe, C., & Ceccarelli, C. 2005, ApJ, 628, 832
Dullemond, C. P., & Dominik, C. 2004, A&A, 417, 159
Edwards, D. P. 1992, GENLN2: A General Line-by-Line Atmospheric Transmittance and Radiance Model, NCAR Technical Note NCAR/TN-367+STR (Boulder, CO: National Center for Atmospheric Research)
Eiroa, C., Oudmaijer, R. D., Davies, J. K., et al. 2002, A&A, 384, 1038
Folha, D. F. M., & Emerson, J. P. 1999, A&A, 352, 517
Furlan, E., Calvet, N., D'Alessio, P., et al. 2005, ApJ, 628, L65
Furlan, E., Hartmann, L., Calvet, N., et al. 2006, ApJS, 165, 568
Goldreich, P., & Ward, W. R. 1973, ApJ, 183, 1051
Goodman, J., & Pindor, B. 2000, Icarus, 148, 537
Goorvitch, D. 1994, ApJS, 65, 535
Hartigan, P., Edwards, S., & Gandhour, L. 1995, ApJ, 452, 736
Hartigan, P., Hartmann, L., Kenyon, S., et al. 1989, ApJS, 70, 899
Hartmann, L., & Stauffer, J. R. 1989, AJ, 97, 873
Hauschildt, P. H., Allard, F., & Baron, E. 1999, ApJ, 512, 377
Herbig, G. H. 1977, ApJ, 214, 747
Hessman, F. V., & Guenther, E. W. 1997, A&A, 321, 497
Hirth, G. A., Mundt, R., & Solf, J. 1997, A&AS, 126, 437
Hodapp, K. W., Walker, C. H., Reipurth, B., et al. 2004, ApJ, 601, L79
Holtzman, J. A., Herbst, W., & Booth, J. 1986, AJ, 92, 1387
Isella, A., Carpenter, J. M., & Sargent, A. I. 2010, ApJ, 714, 1746
Kessler-Silaci, J., Augereau, J. C., Dullemond, C. P., et al. 2006, ApJ, 639, 275
Kitamura, Y., Kawabe, R., & Saito, M. 1996, ApJ, 465, 137
Kitamura, Y., Momose, M., Yokogawa,, et al. 2002, ApJ, 581, 357
Krist, J. E., Stapelfeldt, K. R., Burrows, C. J., et al. 1998, ApJ, 501, 841
Kuhi, L. V. 1974, A&A Suppl., 15, 47
Kulesa, C. A. 2002, PhD thesis, Univ. Arizona
Kurucz, R. L. 1979, ApJS, 40, 1
Kurucz, R. L. 1993, VizieR On-line Data Catalog: VI/39
Mathis, J. S. 1990, ARA&A, 28, 37
Mathis, J. S., Rumpl, W., & Nordsieck, K. H. 1977, ApJ, 217, 425
McCabe, C., Duchêne, G., & Ghez, A. M. 2003, ApJ, 588, L113
McLean, I. S., et al. 1998, Proc. SPIE, 3354, 566
Miyake, K., & Nakagawa, Y. 1995, ApJ, 441, 361
Muzerolle, J., Hartmann, L., & Calvet, N. 1998, AJ, 116, 2965
Muzerolle, J., Hillebrand, L., Calvet, N., et al. 2003, ApJ, 592, 266
Najita, J. R., Carr, J. S., & Mathieu, R. D. 2003, ApJ, 589, 931
Najita, J. R., Crockett, N., & Carr, J. S. 2008, ApJ, 687, 1168
Onge, G. S., & Bastien, P. 2008, ApJ, 674, 1032
Petrov, P. P., Zajtseva, G. V., Efimov, Yu. S., et al. 1999, A&A, 341, 553
Pontoppidan, K. M., Dullemond, C. P., van Dishoeck, E. F., et al. 2005, ApJ, 622, 463
Rebull, L. M., Wolff, S. C., & Strom, S. E. 2004, AJ, 127, 1029
Rettig, T. W., Brittain, S. D., Simon, T., et al. 2006, ApJ, 646, 342
Rothman, L. S., Barbe, A., Benner, D. C., et al. 2003, J. Quant. Spectrosc. Radiat. Transfer, 82, 5
Rothman, L. S., Jacquemert, D., Barbe, A., et al. 2005, J. Quant. Spectrosc. Radiat. Transfer, 96, 139
Safronov, V. S., & Zvjagina, E. V. 1969, Icarus, 10, 109
Scherger, A. A., Wolf, S., Ratzka, T., et al. 2008, A&A, 478, 779
Schmitt, J. H. M. M., & Robrade, J. 2007, A&A, 473, 229
Sneden, C. 1973, PhD thesis Univ. Texas, Austin
Stark, D. P., Whitney, B. A., Stassun, K., et al. 2006, ApJ, 649, 900
St-Onge, G., & Bastien, P. 2008, ApJ, 674, 1032
Testi, L., Bacciotti, F., Sargent, A. I., Ray, T. P., & Eisl o el, J. 2002, A&A, 394, L31
Tilley, D. A., Balsara, D. S., Brittain, S. D., & Rettig, T. 2010, Mon. Not. R. Astron. Soc., 403, 211
Weidenschilling, S. J. 1977, Ap&SS, 51, 153
Weidenschilling, S. J. 1995, Icarus, 116, 433
White, R. J., & Ghez, A. M. 2001, ApJ, 556, 265
Whitney, B. A., Wood, K., Bjorkman, J. E., et al. 2003, ApJ, 598, 1079
Woitke, P., Pinte, C., Tilling, I., et al. 2010, MNRAS, 405, L26
Yokogawa, S., Kitamura, Y., & Momose, M. 2001, ApJ, 552, L59
Youdin, A. N., & Chiang, E. I. 2004, ApJ
Youdin, A. N., & Shu, F. H. 2002, ApJ, 580, 494